

The Physics of Kondo Impurities in Graphene

Lars Fritz

Institut für Theoretische Physik, Universität zu Köln, 50937 Köln, Germany

E-mail: lsfritz@thp.uni-koeln.de

Matthias Vojta

Institut für Theoretische Physik, Technische Universität Dresden, 01062 Dresden, Germany

E-mail: matthias.vojta@tu-dresden.de

Abstract. This article summarizes our understanding of the Kondo effect in graphene, primarily from a theoretical perspective. We shall describe different ways to create magnetic moments in graphene, either by adatom deposition or via defects. For dilute moments, the theoretical description is in terms of effective Anderson or Kondo impurity models coupled to graphene's Dirac electrons. We shall discuss in detail the physics of these models, including their quantum phase transitions and the effect of carrier doping, and confront this with existing experimental data. Finally, we point out connections to other quantum impurity problems, e.g., in unconventional superconductors, topological insulators, and quantum spin liquids.

1. Introduction

The low-temperature behaviour of dilute magnetic impurities in metals, known as the Kondo effect, is a prime example of electron-correlation physics. The impurity's magnetic moment is screened below a temperature T_K by the formation of a many-body singlet with the conduction-electron bath. The Kondo temperature T_K itself depends in a non-analytic fashion on the Kondo coupling and the bath density of states, signalling the breakdown of perturbation theory. Starting with Kondo's work in the 1960s [1], we now have an essentially complete set of theoretical descriptions of the Kondo effect available [2], and agreement between theory and experiment has been established on a quantitative level.

The understanding of the Kondo effect in metals has prompted to investigate similar impurity physics in other settings, with the overarching goal to employ impurities as local probes of the host's properties. This article is devoted to a particularly interesting and timely case, namely the Kondo effect in graphene. Here, the impurity spin interacts with the Dirac fermions of the two-dimensional (2d) sheet of carbon atoms [3, 4, 5, 6]. For a local magnetic impurity in charge-neutral graphene, this results in the Kondo effect being qualitatively different from that in conventional metals, because the bath density of states now vanishes at the Fermi level: Kondo screening is suppressed at small Kondo couplings, and a non-trivial impurity quantum phase transition [7] between an unscreened and a screened impurity spin obtains. In fact, this phase transition has first been discussed for magnetic impurities in unconventional superconductors, where field theories and numerical solutions for the resulting pseudogap Kondo problem have been worked out. Graphene offers the attractive possibility of tuning the chemical potential relative to the Dirac point, such that the crossover between pseudogap and conventional Kondo physics can be accessed in detail. Furthermore, the 2d nature of graphene naturally allows one to employ scanning-probe techniques to locally study impurity physics.

In this article we review the theoretical understanding of the Kondo effect in graphene, together with the current status of experiments. As we will discuss, clear-cut experimental verifications of some of the exciting theoretical ideas are lacking, and we contemplate on possible sources of complications. We also highlight theoretical connections between the Kondo effect in graphene and other quantum impurity problems, such as impurities on the surface of topological insulators.

1.1. Outline

The body of this article is organized as follows: In Sec. 2 we introduce the electronic structure of graphene and review general aspects of magnetic moment formation. We then discuss various possibilities of experimentally realizing magnetic moments coupled to graphene sheets, together with the relevant microscopic descriptions. Quite generically, this will lead to versions of the pseudogap Kondo model, whose theoretical treatment is discussed in some detail in Sec. 3. We describe the phase diagram,

the quantum field theories and resulting critical properties, the crossovers for finite chemical potential, and the implications for Kondo physics in graphene. Sec. 4 confronts these theoretical results with experimental data obtained on impurity-doped graphene. Various real-world complications and their influence on the interpretation of experiments will be discussed as well. Finally, in Sec. 5 we discuss quantum impurity problems which are relatives of the graphene Kondo problem, thereby highlighting the generality of the theoretical concepts developed in the field.

2. Magnetic impurities in graphene

In this section, we discuss how to realize magnetic impurity moments coupled to graphene conduction electrons. To set the stage we first summarize basic aspects of both the electronic structure of graphene and the formation of local moments in general.

2.1. Electronic structure of graphene

Graphene is a 2d hexagonal arrangement of carbon atoms [3, 4, 5, 6]. While the sp^2 orbitals hybridize to yield the σ orbitals which are electrically inert and responsible for the remarkable mechanical robustness of graphene, its electronic structure is determined by the p_z orbitals which form the π -bonds. This allows electron hopping between adjacent atoms and gives rise to a kinetic energy described by the following tight-binding Hamiltonian [8]:

$$\mathcal{H}_0 = -t \sum_{\langle i,j \rangle, \sigma} \left(a_{\sigma,i}^\dagger b_{\sigma,j} + \text{h.c.} \right) - t' \sum_{\langle\langle i,j \rangle\rangle, \sigma} \left(a_{\sigma,i}^\dagger a_{\sigma,j} + b_{\sigma,i}^\dagger b_{\sigma,j} + \text{h.c.} \right) \quad (1)$$

Here, $a_{\sigma,i}$ and $b_{\sigma,j}$ are annihilation operators for electrons on sites i, j of the two sublattices A and B , see Fig. 1 a. The sums run over pairs of nearest and next-nearest neighbours, respectively, with the hopping matrix elements given by $t = 2.8 \text{ eV}$ and $t' \approx 0.1t$. Diagonalizing the Hamiltonian (1) yields two dispersive bands

$$E_{\pm, \vec{k}} = \pm t \sqrt{3 + f_{\vec{k}}} - t' f_{\vec{k}} \quad \text{with} \\ f_{\vec{k}} = 2 \cos \left(\sqrt{3} k_y a_1 \right) + 4 \cos \left(\frac{\sqrt{3}}{2} k_y a_1 \right) \cos \left(\frac{3}{2} k_x a_1 \right), \quad (2)$$

where $a_1 = 1.42 \text{ \AA}$ denotes the bond length, i.e. the distance between neighbouring carbon atoms. The two bands (dubbed π^* and π) touch at the two inequivalent wavevectors $K = \left(\frac{2\pi}{3a_1}, \frac{2\pi}{3\sqrt{3}a_1} \right)$ and $K' = \left(\frac{2\pi}{3a_1}, -\frac{2\pi}{3\sqrt{3}a_1} \right)$, see Fig. 1a. Close to K and K' the dispersion is found to be linear:

$$E_{\pm, \vec{q}} = \pm v_F |\vec{q}| \quad (3)$$

where $\vec{q} = \vec{k} - \vec{K}$ (or \vec{K}'), $v_F = 3ta_1/2 \approx 1.1 \times 10^6 \text{ m/s}$, and an additional constant proportional to t' has been omitted in E_{\pm} .

For charge-neutral graphene, the electronic system is half-filled, i.e. in the ground state all E_- states are filled while the E_+ states are empty, such that the Fermi level

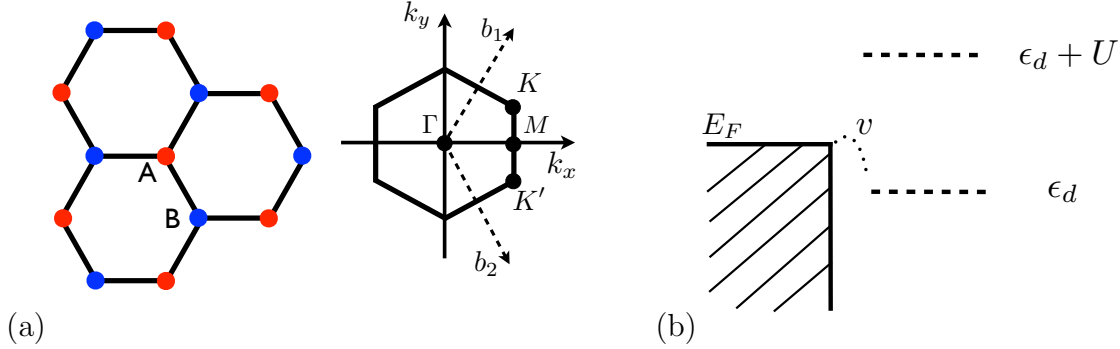


Figure 1. (a) Honeycomb lattice of graphene with two inequivalent carbon atoms per unit cell, A and B , and its hexagonal Brillouin zone. The points K and K' are the touching points of the E_{\pm} bands. (b) Sketch of the AIM: A local spin-degenerate level with energy ϵ_d is hybridized via v with a sea of conduction electrons. Local double occupancy costs the Coulomb energy U .

coincides with the band energy at K and K' . Then Eq. (3) is the dispersion of the system's low-energy excitations which admit a description in terms of two-component massless Dirac equations, one for each of the valleys at K and K' [5]. The 2d linear dispersion results in a low-energy density of states (DOS) per spin which vanishes linearly at the Fermi level,

$$\rho(\omega) = \frac{2}{\sqrt{3}\pi t^2} |\omega|, \quad (4)$$

rendering graphene a semimetal. (Here and in the following, energies are measured relative to the Fermi level, unless otherwise noted.)

2.2. Local-moment formation in metals

The general mechanism of local-moment formation in metals was formulated by Anderson in 1961 [9]: a strong Coulomb interaction U between electrons in a spin-degenerate doublet of levels, d_{σ} , can freeze out charge fluctuations, leaving behind an effective spin degree of freedom interacting with the spin density of the conduction electrons, $c_{\vec{k}\sigma}$. Typically, such a situation is realized for impurity atoms with partially filled d or f shells. The corresponding minimal model is known as the Anderson impurity model (AIM):

$$\mathcal{H} = \sum_{\vec{k},\sigma} \epsilon_{\vec{k}} c_{\vec{k}\sigma}^{\dagger} c_{\vec{k}\sigma} + \epsilon_d \sum_{\sigma} n_{d\sigma} + U n_{d\uparrow} n_{d\downarrow} + \sum_{\vec{k},\sigma} \left(v_{\vec{k}} c_{\vec{k}\sigma}^{\dagger} d_{\sigma} + \text{h.c.} \right) \quad (5)$$

where $n_{d\sigma} = d_{\sigma}^{\dagger} d_{\sigma}$. Moment formation can be understood starting from the atomic limit, $v_{\vec{k}} = 0$. For $\epsilon_d < E_F$ and $\epsilon_d + U > E_F$ the d level prefers single occupancy, such that charge fluctuations are frozen out and an effective spin 1/2 degrees of freedom remains. Upon switching on the hybridization $v_{\vec{k}}$, the so-formed local moment becomes entangled

with the conduction electrons. It is convenient to convert the momentum dependence of $v_{\vec{k}}$ and $\epsilon_{\vec{k}}$ into an energy-dependent hybridization function

$$\Delta(\omega) = \sum_{\vec{k}} \frac{|v_{\vec{k}}|^2}{\omega - \epsilon_{\vec{k}}} \quad (6)$$

which fully characterizes the impurity's bath. For small $v_{\vec{k}}$, one can utilize a Schrieffer-Wolff transformation to derive an effective Kondo model from Eq. (5), describing the interaction of the local-moment spin with the conduction electrons, see Sec. 3.

2.3. Magnetic adatoms on graphene

We turn to the graphene-specific discussion of how to realize magnetic impurity moments with sizeable electronic coupling to the host electrons. An apparently straightforward route is to place a magnetic ad-atom onto the graphene sheet, e.g., using the manipulation capabilities of a scanning tunneling microscope (STM). For magnetic atoms like Fe or Co on the surface of conventional metals, this route has been successfully used in the past to study local spectral signatures of Kondo screening using STM techniques [10].

In the following we discuss theoretical aspects of such adatoms on graphene; experiments will be reviewed in Sec. 4. The key questions for a quantitative understanding of the adatom's magnetism are:

- (i) At which lattice position does the adatom adsorb? For graphene, possible high-symmetry locations are shown in Fig. 2a and labeled h (hollow, in the center of a hexagon), b (bridge, on a bond between two C atom), and t (on top of a C atom).
- (ii) What is the spin state of the impurity adatom?
- (iii) In an Anderson-model description, how are the impurity levels hybridized with conduction electrons?

All these question turn out vital for the presence or absence of the Kondo effect. Answering these questions is highly non-trivial: While symmetries provide important constraints on possible models [12, 13, 14, 15, 16], an in-depth analysis requires ab-initio calculations, typically using variants of density-functional theory (DFT).[‡]

2.3.1. Co. For Co atoms on an isolated graphene sheet, DFT calculations using the generalized gradient approximation (GGA) found that the preferred adsorption is at site h with spin $S = 1/2$ [12]. However, upon accounting for the local Coulomb repulsion U and Hund's-rule coupling J within the GGA+ U method, this picture was modified: While for values of $U = 2\text{eV}$ and $J = 0.9\text{eV}$ the h position and $S = 1/2$ were still favoured, increasing U to 4eV selected the t position and $S = 3/2$ [12, 17]. As U can only be estimated to be in the range $2\text{eV} < U < 4\text{eV}$, a clear-cut answer was missing

[‡] Notably, even for the “classic” situation of Fe atoms in gold or silver, the correct model description has only been determined very recently [11] to be a spin- $\frac{3}{2}$ three-channel Kondo model.

here, but the case of a spin $S = 1/2$ on the h site was advertised as the most promising candidate for observing Kondo physics.

In an alternative calculation, based on DFT augmented by a dynamical treatment of the 3d levels in the framework of the one-crossing approximation, dubbed GGA+OCA, a $S = 3/2$ configuration on the t position was found to be most stable [18]. Here, the authors argued in favour of a Kondo effect with full screening, as three conduction-band channels coupled to the impurity spin. Finally, in a refined quantum-chemical calculation [19] based on a complete active-space self-consistent field approach, albeit on small clusters, it was found that Co in an h position favours a higher-spin state of $S = 3/2$.

Overall, the situation concerning Co adatoms is unclear at present, and more theory work is called for. Specifically, the effect of the substrate, which possibly influences the adatom's behaviour, has not been investigated so far.

2.3.2. NiH. Recently, it has been proposed that a more promising route towards realizing the Kondo effect could be provided by using NiH as adsorbing molecule [17]. From GGA+U, the molecule favors a $S = 1/2$ state in the h position [17].

2.3.3. Effective model. As in Sec. 2.2, the physics of a localized impurity level hybridized with graphene electrons can be described by an Anderson impurity model, § which then may be mapped onto an effective Kondo model, see Sec. 3.

For a spin- $\frac{1}{2}$ Co atom in the h position, it was argued [12] that, due to an approximate orbital degeneracy, the impurity behaviour at elevated energies corresponds to that of an SU(4) Kondo effect. The orbital splitting is roughly 60 meV, such that a standard single-channel SU(2) $S = 1/2$ Kondo or Anderson model applies at energies below this scale, albeit with a non-standard hybridization function $\Delta(\omega)$. The latter was calculated in Ref. [12] and is reproduced in Fig. 2b. It vanishes near the Dirac-point energy (set to zero here) according to

$$\text{Im } \Delta(\omega) \propto |\omega|, \quad (7)$$

a behaviour inherited from the graphene DOS, while for higher energies there is sizeable particle-hole asymmetry. Both features turn out vital for the Kondo effect, see Sec. 3.2. It can be expected on symmetry grounds that this effective model with a similar hybridization function applies to NiH on the h site as well.

2.4. Defect-induced moments in graphene

A different route towards magnetic impurities in graphene is via point defects which themselves induce moments. Relevant defects include vacancies, created e.g. by irradiation [22, 23], and hydrogen and fluorine adatoms.

§ The mean-field solution of the Anderson model for charge-neutral graphene has been discussed in Ref. [20]; for aspects of the full solution see Ref. [21] and Sec. 3.

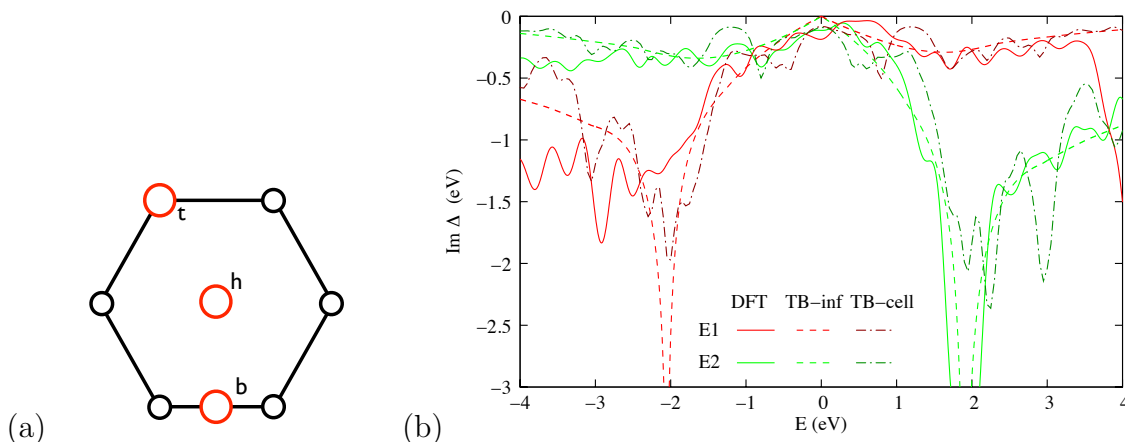


Figure 2. (a) Possible high-symmetry adsorption sites of ad-atoms on the graphene sheet, denoted by h (hollow), t (top), and b (bridge). (b) Hybridization function of the active impurity level of a Co atom in the h position in a spin state of $S = 1/2$ [12]. Solid: DFT result, dashed: tight-binding fit. E1, E2 refer to different orbital configurations, with E1 being lower in energy (taken from Ref. [12]).

2.4.1. π -orbital magnetic moment. Removing a single site from the π -electron tight-binding Hamiltonian in Eq. (1) induces a single localized state *at* the Dirac-point energy for $t' = 0$, which becomes a quasi-localized resonance near the Dirac-point energy for non-zero t' [5, 24]. Consequently, it has been proposed that, upon including Coulomb interactions, a magnetic moment may be formed in this localized state, i.e. in the vicinity of the vacancy. However, in real graphene the lattice near the vacancy will reconstruct, such that determining the proper effective model requires ab-initio studies.

Notably, the results of those studies are again controversial. Initially, local-moment formation for a vacancy was confirmed using DFT, however, the coupling to the conduction electrons was argued to be ferromagnetic [25], such that no Kondo effect can be expected. A similar conclusion was drawn from a study using dynamical mean-field theory (DMFT) [26] where a Curie-type susceptibility was found indicative of a free moment. In contrast, for an H atom adsorbed on top of a C atom, Ref. [27] argued that the physics can be described by a single $S = 1/2$ impurity coupled antiferromagnetically to the environment, such that screening with sizable Kondo temperature should be possible. Finally, a more recent DFT calculation [28] for a finite concentration of H adatoms concluded that, while there can be localized σ -orbital moments, π -orbital moments only occur for the unlikely situation of hydrogenation of all dangling σ bonds. This paper pointed out the importance of considering both σ and π bonds and their reconstruction around a vacancy.

In any case, if a π moment forms then it can be expected that its coupling to the conduction electrons is described by an Anderson/Kondo model with a pseudogap hybridization function as in Eq. (7), possibly with a large particle-hole asymmetry at higher energies due to potential scattering. The physics of this pseudogap Kondo model will be discussed in detail in Sec. 3.

2.4.2. σ -orbital magnetic moment. An interesting alternative is to consider the carbon's σ orbitals. While local-moment formation driven by Coulomb interaction is possible here as well, the obstacle is that – for flat graphene – the hybridization between σ and π orbitals vanishes, i.e. such a moment would not couple to the conduction electrons. However, hybridization of σ and π orbitals becomes possible once structural deviations from the flat geometry are included, i.e. by corrugations of the graphene sheet around the impurity site.

Ref. [29] investigated vacancies and σ -orbital moments from an LDA+U perspective. It was found that $S = 1/2$ or $S = 1$ σ moments emerge, which can have sizeable single-channel hybridization to the π electrons upon including rippling, which occurs under small isotropic compression around reconstructed vacancies. Interestingly, the hybridization function within an effective Anderson model was found to be low-energy divergent according to

$$\text{Im } \Delta(\omega) \propto \frac{1}{|\omega| \ln^2 |\omega/D|}, \quad (8)$$

where D is the bandwidth, providing a high-energy cutoff. In that situation the Kondo temperature can largely be enhanced due to the massive density of states at low energies [29, 30], but detailed studies of this model are not available.

3. The pseudogap Kondo problem

We now discuss the rich physics of the so-called pseudogap Kondo model, relevant to low-energy behaviour of magnetic moments in graphene. We will restrict our attention to the case of a spin $S = 1/2$ coupled to a single screening channel; the two-channel version will be briefly mentioned in Sec. 4.2.

3.1. The pseudogap Kondo model

The standard Kondo Hamiltonian [2] reads

$$\mathcal{H} = \sum_{\vec{k}, \sigma} \epsilon_{\vec{k}} c_{\vec{k}\sigma}^\dagger c_{\vec{k}\sigma} + V_0 \sum_{\vec{k}, \vec{k}', \sigma} c_{\vec{k}\sigma}^\dagger c_{\vec{k}'\sigma} + J_0 \vec{S} \cdot \vec{s}_0, \quad (9)$$

where the notation follows Sec. 2.2, \vec{S} is the impurity spin $S = 1/2$, and $\vec{s}_0 = \frac{1}{2} \sum_{\vec{k}, \vec{k}'} c_{\vec{k}\sigma}^\dagger \vec{\tau}_{\sigma\sigma'} c_{\vec{k}'\sigma'}$ is the conduction-electron spin density at the impurity site, with $\vec{\tau}$ the vector of Pauli matrices. The Kondo coupling J_0 and the potential-scattering strength V_0 characterize the impurity. If the Kondo model is derived from the more general Anderson model, Eq. (5), in the limit of small charge fluctuations, second-order perturbation theory yields [2]:

$$J_0 = 2v^2 \left(\frac{1}{|\epsilon_d|} + \frac{1}{|U + \epsilon_d|} \right), \quad V_0 = \frac{v^2}{2} \left(\frac{1}{|\epsilon_d|} - \frac{1}{|U + \epsilon_d|} \right) \quad (10)$$

where $v_{\vec{k}} \equiv v$ has been assumed. Note that $V_0 \neq 0$ breaks particle–hole symmetry if the host DOS is particle–hole symmetric, $\rho(\omega) = \rho(-\omega)$.||

|| This symmetry is not obeyed even for neutral graphene due to finite next-neighbor hopping t' .

For a metallic host, the DOS $\rho(\omega)$ is finite at the Fermi level. Then, for antiferromagnetic $J > 0$ the impurity spin is screened below the so-called Kondo temperature T_K . For a flat conduction-band DOS, $\rho(\omega) = \rho_0$, one finds [2]:

$$T_K = \sqrt{DJ_0} e^{-1/(J_0\rho_0)}. \quad (11)$$

Importantly, in this metallic Kondo problem, the crossovers at finite energies and temperatures are characterized by the *single* scale T_K . For instance, the impurity susceptibility displays single-parameter scaling: $\chi_{\text{imp}}(T)$ is a universal function of T/T_K only, and does not depend on further microscopic details.

In the following, we will instead concentrate on the case of a pseudogap DOS,

$$\rho(\omega) = \frac{1+r}{2D^{r+1}} |\omega|^r \Theta(|\omega| - D) \quad (12)$$

with $r > 0$. This is the situation of a semimetal with vanishing DOS at the Fermi level. Consequently, the tendency toward Kondo screening is reduced, such that no screening occurs at small Kondo coupling J_0 . As a result, a quantum phase transition between phases without and with screening occurs upon increasing J_0 [7, 31], as discussed in detail below. Importantly, the form of the DOS (12) with $r = 1$ is relevant for both *d*-wave superconductors and charge-neutral graphene at low energies. We note that the implications of the vanishing DOS for the x-ray edge problem in graphene and the associated Anderson orthogonality catastrophe were discussed in Ref. [32].

3.2. Phase diagram

Despite its simplicity, the pseudogap Kondo model has an extraordinarily rich phase diagram, first determined by Gonzalez-Buxton and Ingersent [21] using Wilson's numerical renormalization group (NRG) technique. The physics depends not only on J_0 and the exponent r of the low-energy DOS, but also on the presence or absence of particle-hole symmetry. [We recall that particle-hole symmetry requires *both* $\rho(\omega) = \rho(-\omega)$ in the host and $U = -2\epsilon_d$ in the AIM (5).]

Thanks to both numerical [21, 33, 34, 35] and perturbative [36, 37] RG studies, the phases and phase transitions of the pseudogap Kondo and Anderson models are by now fully understood, and will be summarized below. This discussion, restricted to $r > 0$, mainly follows Ref. [21] and is cast in the language of RG flows and fixed points. We start by listing the fixed points of the problem. For brevity, we will use the acronyms of Ref. [21] for both the phases and their stable fixed points.

Local-moment phase **LM**. Here the impurity moment is asymptotically decoupled from the host and behaves like a free local moment, i.e. it has a residual entropy $S_{\text{imp}} = \ln 2$.

Symmetric strong-coupling phase **SSC**. This phase corresponds to Kondo screening in the presence of particle-hole symmetry and is the generalization of the metallic Kondo-screened phase to finite r . Interestingly, SSC is characterized by a residual entropy $S_{\text{imp}} = 2r \ln 2$, which means the impurity moment is only partially screened.

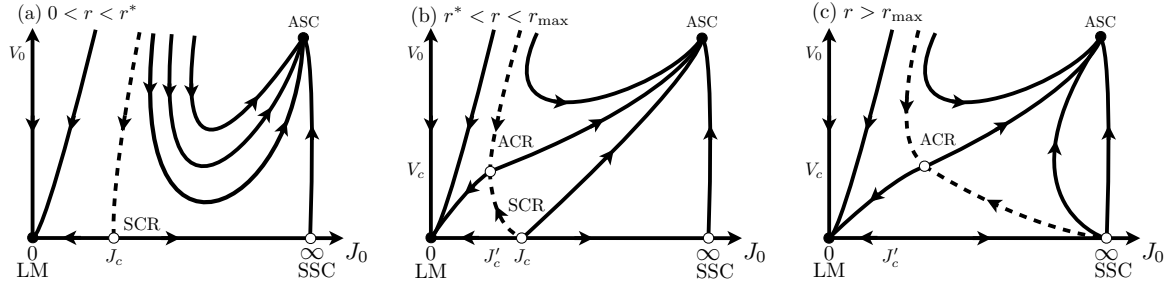


Figure 3. Schematic RG flow diagrams for the pseudogap Kondo model [21] in the plane spanned by the Kondo coupling J_0 and the potential scattering V_0 , the latter measuring particle–hole asymmetry. The flow topology changes qualitatively as function of r , as shown in the three panels, with $r^* = 0.375 \pm 0.002$ and $r_{\max} = 1/2$, for details see text. Full dots denote stable fixed points, while open dots are critical fixed points. Dashed lines denote separatrices, i.e., phase boundaries.

Asymmetric strong-coupling phase ASC. In the absence of particle–hole symmetry and for $r > 0$, full screening with $S_{\text{imp}} = 0$ obtains at ASC, which is maximally particle–hole asymmetric.

Critical points SCR and ACR. The pseudogap Kondo problem has two distinct critical fixed points, distinguished by their symmetry under particle–hole transformation and denoted “symmetric critical” (SCR) and “asymmetric critical” (ACR), respectively. They both exist over a restricted range of r values.

As deduced from the numerical solution of the pseudogap Kondo model [21], the topology of the phase diagram changes *qualitatively* as the bath exponent r is varied. Different phase diagram topologies are observed in three regimes, see Fig. 3.

a) $0 < r < r^* = 0.375 \pm 0.002$

- (i) For particle–hole symmetry, a critical coupling J_c , associated with SCR, separates LM from SSC. For initial values $J < J_c$ the flow is directed towards LM, whereas for $J > J_c$ the flow is directed towards SSC.
- (ii) For finite particle–hole asymmetry, i.e. $V_0 \neq 0$, there is a separatrix which separates the flow towards LM from the flow towards ASC.
- (iii) Particle-hole asymmetry is irrelevant at LM and SCR while it is relevant at SSC where it drives the flow towards ASC. SCR is thus a multicritical fixed point.

b) $r^* < r < r_{\max} = 1/2$

- (i) For $V_0 = 0$ there still exists a critical coupling which separates LM from SSC.
- (ii) SCR is now unstable w.r.t. particle–hole asymmetry, and a new asymmetric critical fixed point ACR emerges, controlling the transition between LM and ASC.

c) $\mathbf{r} > \mathbf{r}_{\max}$

- (i) SCR merges with SSC, such that there is no Kondo screening at particle-hole symmetry, irrespective of the strength of the Kondo coupling J_0 .
- (ii) Screening is possible for finite asymmetry, where ACR continues to control the LM-ASC transition.
- (iii) The critical exponents at ACR take trivial values for $r > 1$, such that $r = 1$ – the case relevant for charge-neutral graphene – acts as an upper-critical dimension [21, 35, 36].

d) $-\mathbf{1} < \mathbf{r} < \mathbf{0}$ This regime can possibly be realized in the case of reconstructed vacancies in graphene [29] but was analyzed more generally in Ref. [30]. SSC is stable, and a critical point ACR separates SSC from a newly emerging fixed point ALM, located at $J_0 = 0$ and $V_0 = \infty$. In the following we will, however, not discuss $r < 0$ in any detail.

Notably, the pseudogap Kondo and Anderson models share identical fixed points and quantum phase transitions [21]. This observation can be rationalized within the effective field theories described in Sec. 3.4 below.

3.3. Slave-boson mean-field theory

A simple and popular approach to the Kondo model in Eq. (9) is the slave-boson mean-field theory [2, 38]; a very similar mean-field theory can be applied to the Anderson model (5). In this approach, formally justified in a limit where the spin symmetry is taken to be $SU(N)$ with $N \rightarrow \infty$, the Kondo interaction is decoupled by a Hubbard-Stratonovich field which is then approximated to be static. This results in a renormalized free-particle Hamiltonian which reproduces salient low-temperature properties of a Kondo-screened impurity in a metal.

The slave-boson approach has been applied to the pseudogap Kondo model in numerous of papers [16, 20, 31, 39, 40, 41, 42, 43, 44]. It reproduces the existence of a quantum phase transition at $r > 0$, however, the critical properties of this transition are only correctly captured for small r . For larger r including the graphene case $r = 1$, the slave-boson method becomes unreliable. It is not sensitive to the subtle effects of particle-hole symmetry breaking: It fails to describe the properties near the ACR fixed point, and it incorrectly predicts a phase transition for $r > 1/2$ even in the particle-hole symmetric case. Therefore, quantitative calculations require numerical methods such as NRG.

3.4. Critical field theories

The complicated topology of the RG flow, Fig. 3, suggests that different field theories are required to describe the critical properties near the SCR and ACR fixed points. Such field theories have been worked out in detail in Refs. [36, 37] and provide an

essentially complete analytical understanding of the pseudogap Anderson and Kondo models. Interestingly, none of these field theories is of conventional (i.e. bosonic) Landau-Ginzburg-Wilson type; instead all are of genuinely fermionic character and are formulated in the degrees of freedom of either the Kondo or the Anderson model.

In the following we shall summarize the three relevant critical theories. As will become clear, only the third will be appropriate to describe the quantum phase transition of Kondo impurities in charge-neutral graphene, where $r = 1$. When specifying flow equations from perturbative RG, we will assume a symmetric pseudogap density of states as in Eq. (12). The effect of a high-energy particle-hole asymmetry in the DOS can be absorbed in the impurity part of the Hamiltonian, e.g., the potential scattering term of the Kondo model. This can be rationalized within RG, where integrating out the particle-hole asymmetric piece of the bath at high energies yields an effective model with particle-hole symmetric bath at low energies and a renormalized impurity Hamiltonian, where in particular the particle-hole asymmetry is accumulated.

3.4.1. SCR: Kondo model. For small r , an efficient description of the physics at SCR is obtained via the Kondo model itself, Eq. (9). A perturbative expansion can be performed in J_0 and V_0 around the LM fixed point where $J_0 = V_0 = 0$ [31, 39, 35, 37]. As is standard practice, we introduce dimensionless couplings j and v , for details see Ref. [37]. Power counting reveals that both couplings are marginal for $r = 0$ and irrelevant for $r > 0$, $\dim[j] = \dim[v] = -r$. The one-loop flow equations read

$$\frac{dj}{d \ln D} = rj - j^2 \quad \text{and} \quad \frac{dv}{d \ln D} = rv, \quad (13)$$

where D denotes the running UV cutoff, initially set by the width of the host band. Eq. (13) yields a critical fixed point (SCR) at $j^* = r + \mathcal{O}(r^2)$, $v^* = 0$, which separates the flows towards weak and strong coupling. Controlled calculations near SCR are therefore possible in a double expansion in r and j . Potential scattering is irrelevant at SCR and consequently does not play a role for leading critical exponents.

Comparing these properties with the numerically deduced flows in Fig. 3, it is clear that this Kondo description of SCR is appropriate for $0 < r < r^*$. It does, however, not capture the physics for $r > r^*$ where v becomes a relevant perturbation at the SCR fixed point, and it is obviously inappropriate for the graphene case $r = 1$.

A perturbative calculation of static critical properties of SCR using the Kondo expansion indeed shows excellent agreement with NRG results for small r [37]. Crossover functions and dynamical properties have been studied as well, using a combination of perturbative RG and Callan-Szymanzik equations [45], and agreement with NRG results has been found where those are available. ¶

¶ In the quantum-relaxational finite-temperature regime of $\omega \ll T$ numerical studies are notoriously difficult. Here, the Callan-Szymanzik results [45] disagree with numerical data [46]: the latter indicate that the imaginary part of local Green function (or T matrix) $G''(\omega, T)$ multiplied by T^r goes to a non-zero constant, i.e. $T^r G''(\omega/T \rightarrow 0) = c \neq 0$, while the former suggests that it goes to zero.

3.4.2. SCR: Symmetric Anderson model. The Anderson impurity model, originally introduced as model for local-moment formation (Sec. 2.2), turns out to provide the relevant degrees of freedom to describe pseudogap Kondo criticality for all $r > 0$ [37]. This generically implies that critical fluctuations occur not only in the spin channel, but also in the charge channel [47].

To discuss the critical behaviour near SCR, we consider a symmetric AIM, Eq. (5) with $\epsilon_d = -U/2$, a momentum-independent hybridization v , and a particle-hole symmetric bath DOS as in Eq. (12). The point $\epsilon_d = U = v = 0$ is referred to as the free-impurity fixed point (FImp), whereas the parameter sets $v = 0$ and $\epsilon_d = -U/2 = \pm\infty$ correspond to doubly degenerate local-moment states in the charge and spin channel, respectively. Therefore $v = 0$, $\epsilon_d = -\infty$ can be identified with the LM fixed point, while $v = 0$, $\epsilon_d = \infty$ is dubbed LM'.

Notably, the Anderson model is exactly solvable for any v at $U = 0$, known as resonant-level model. In the particle-hole symmetric case, its low-energy physics can be identified with that of the SSC fixed point introduced above:⁺ its properties correspond to a partial screening of the impurity degrees of freedom, with a residual entropy of $S_{\text{imp}} = 2r \ln 2$ [21, 37].

A perturbative expansion is now possible in U around the SSC fixed point. The scaling dimension of the renormalized Coulomb interaction u at SSC is found to be $\text{dim}[u] = -\bar{r} = -(1 - 2r)$. The RG flow of u to two-loop order reads [37]

$$\frac{du}{d \ln D} = (1 - 2r)u - \frac{3(\pi - 2 \ln 4)}{\pi^2} u^3. \quad (14)$$

This flow, together with the trivial flow near LM, LM', and FImp is illustrated in Fig. 4 [37]. For all $r > 0$, LM is a stable fixed point, while SSC is stable only for $r < r_{\text{max}}$, as can be seen from Eq. (14). Therefore, a critical fixed point (SCR) emerges for $0 < r < r_{\text{max}}$, Fig. 4b, consistent with Fig. 3. Its properties can now be accessed in a double expansion in \bar{r} and u , and Eq. (14) yields for the fixed-point coupling at $u^{*2} = \frac{\pi^2}{3(\pi - 2 \ln 4)} \bar{r}$. A perturbative calculation of static critical properties again yields excellent agreement with NRG results, here for $r \lesssim r_{\text{max}}$ [37].

Owing to particle-hole symmetry, the behaviour at $\epsilon \geq 0$ is formally identical to that at $\epsilon \leq 0$, Fig. 4, with the latter describing spin-Kondo physics while the former corresponds to charge-Kondo physics. Finally, we note that particle-hole symmetry breaking can be studied perturbatively for small \bar{r} , and is found to be relevant at both SSC and SCR fixed points, again consistent with Fig. 3. In fact, estimating its scaling dimension at SCR as function of r , one finds that particle-hole symmetry breaking changes from being relevant to being irrelevant once r is reduced below $r \approx 0.40$ [48] – this value can be identified with r^* , Fig. 3.

3.4.3. ACR: Asymmetric Anderson model. We now turn to the ACR fixed point present for $r > r^*$. This is ultimately relevant for understanding the Kondo effect

⁺ In the metallic case, $r = 0$, it is known that the resonant-level model is the correct fixed-point theory for a Kondo-screened impurity spin.

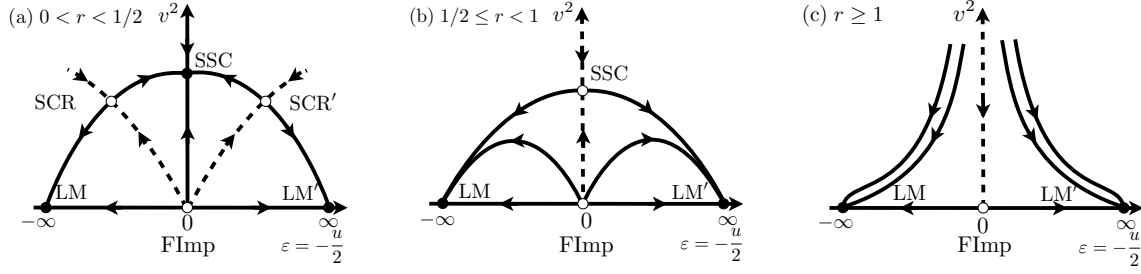


Figure 4. RG flow diagrams for the particle–hole symmetric Anderson model [37], in the plane spanned by the level energy $\epsilon = -u/2$ and the hybridization v^2 . Symbols are as in Fig. 3, with LM and LM' corresponding to local moments formed in the spin or charge channel; the flow of u near SSC is in Eq. (14). (a) $0 < r < 1/2$: The critical fixed point SCR (SCR') divides the flow to LM (LM') from that to SSC. (b) $1/2 \leq r < 1$: SCR and SCR' merge with SSC as $r \rightarrow 1/2^-$, such that SSC is now unstable. (c) $r \geq 1$: SSC merges with FImp at $\epsilon = v = 0$ as $r \rightarrow 1^-$. For all $r \geq 1/2$, LM and LM' are the only stable phases in the presence of particle–hole symmetry. For details see text and Ref. [37].

in graphene, because there $r = 1$ at charge neutrality, and $t' \neq 0$ breaks particle–hole symmetry already on the level of the band structure.

It was realized in Ref. [36] that the critical theory for ACR is that of a level crossing of a many-body singlet and a many-body doublet, minimally coupled to conduction electrons. Using the notation of Ref. [36, 37], its Hamiltonian can be written as

$$\mathcal{H} = \sum_{\vec{k}, \sigma} \epsilon_{\vec{k}} c_{\vec{k}\sigma}^\dagger c_{\vec{k}\sigma} + \epsilon_0 |\sigma\rangle \langle \sigma| + g_0 [|\sigma\rangle \langle s| c_\sigma(0) + \text{h.c.}] \quad (15)$$

where $|\sigma\rangle = |\uparrow\rangle, |\downarrow\rangle$ and $|s\rangle$ represent the three allowed impurity states. ϵ_0 is the tuning parameter (“mass”) of the QPT, i.e. the (bare) energy difference between doublet and singlet states. The QPT occurs at some $\epsilon_0 = \epsilon_c$, with screening present for $\epsilon_0 > \epsilon_c$. Remarkably, this theory is identical to a maximally particle–hole asymmetric Anderson impurity model, Eq. (5), where the doubly occupied state has been projected out, $U \rightarrow \infty$, and (ϵ_0, g_0) in Eq. (15) have been identified with (ϵ_d, v) in Eq. (5).

In this model, the point $\epsilon_0 = g_0 = 0$ is dubbed valence-fluctuation fixed point (VFI). As above, $g_0 = 0, \epsilon_0 = -\infty$ corresponds to LM, while $g_0 = 0, \epsilon_0 = \infty$ describes a fully screened and particle–hole asymmetric singlet state, to be identified with ASC.

A perturbative expansion is now possible in g_0 around VFI. Power counting yields the scaling dimension of the renormalized hybridization $\dim[g] = \tilde{r} = \frac{1-r}{2}$. The one-loop flow equations for g and the renormalized mass ϵ read

$$\begin{aligned} \frac{dg}{d \ln D} &= -\tilde{r}g + \frac{3}{2}g^3 \\ \frac{d\epsilon}{d \ln D} &= -\epsilon - g^2 + 3g^2\epsilon, \end{aligned} \quad (16)$$

results to two-loop order can be found in Ref. [37]. The RG flow is shown in Fig. 5 – this flow has strong similarity to that of the standard Landau-Ginzburg model. The

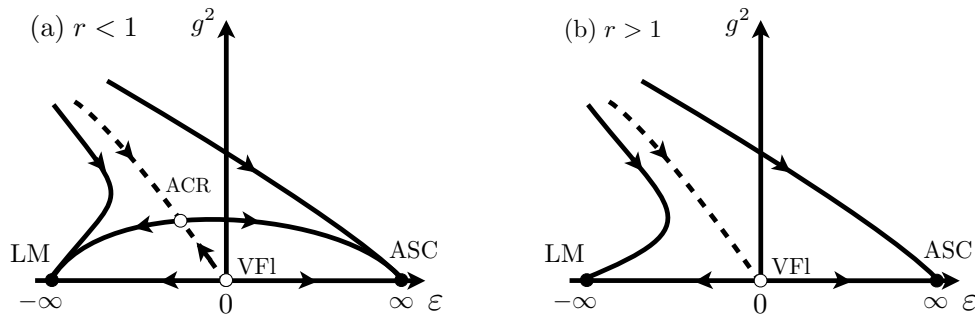


Figure 5. RG flow for the asymmetric Anderson model [36, 37] in the ϵ - g^2 plane, obtained from Eq. (16) (a) $r < 1$: The critical fixed point ACR separates the flow towards LM from that to ASC. (b) $r \geq 1$: ASC merges with VFI as $r \rightarrow 1^-$, which describes a level crossing with perturbative corrections. The behaviour near $r = 1$ is similar to that of the Landau-Ginzburg model near $d = 4$, with VFI and ASC corresponding to the Gaussian and Wilson-Fisher fixed points, respectively.

fact that g is relevant for $r < 1$ and irrelevant for $r > 1$ allows us to identify $r = 1$ as an upper-critical dimension of the pseudogap Kondo problem, akin to $d = 4$ in the Landau-Ginzburg theory. For $r < 1$ a non-trivial fixed point (ACR) emerges at $g^{*2} = \frac{2}{3}\tilde{r}$ and $\varepsilon^* = -\frac{2}{3}\tilde{r}$, Fig. 5a, similar to the celebrated Wilson-Fisher fixed point. Critical properties, evaluated in a double expansion in \tilde{r} and g , again agree well with NRG results [37]. In contrast, for $r \geq 1$ in Fig. 5b, we have “Gaussian” behaviour controlled by the VFI fixed point, which here corresponds to a simple level crossing with corrections captured by plain perturbation theory in g_0 . In the case $r = 1$, relevant to charge-neutral graphene, this perturbation theory is logarithmically divergent at criticality and needs to be resummed, as is standard at the upper critical dimension.

The structure of the critical theory (15) implies that spin and charge fluctuations are strongly coupled, i.e. suitably defined observables in the charge sector become critical at the Kondo quantum phase transition controlled by ACR [36, 47].

3.5. Finite carrier concentration

For graphene away from charge neutrality, $\mu \neq 0$, the DOS at the Fermi level is finite, and consequently a magnetic impurity described by the Kondo model (9) will be screened in the low-temperature limit for any value of the Kondo coupling J_0 [49, 50, 51]. To be specific, let us consider a Kondo model (9) with bath DOS

$$\rho(\omega) = \frac{1+r}{2D^{r+1}} |\omega - \mu|^r \Theta(|\omega - \mu| - D). \quad (17)$$

In the limit of small J_0 the corresponding Kondo temperature will be exponentially small according to $\ln T_K \propto -\frac{1}{|\mu|^r}$, but in general T_K needs to be calculated numerically, as the simple equation (11) is no longer applicable due to the strong energy dependence of the DOS.

On general grounds, one expects that the presence of the quantum phase transition at $J_0 = J_c$, $\mu = 0$ influences the behaviour at finite μ as well, Fig. 6a. In this quantum critical regime, heuristic scaling arguments suggest $T_K = \kappa|\mu|$ with a *universal* constant κ depending on r only. This problem can be tackled by generalizing the RG equations (16) obtained for ACR to a finite chemical potential [50]:

$$\begin{aligned} \frac{dg}{d \ln D} &= -\frac{1-r}{2}g + \frac{g^3}{2}F_1\left(\frac{\mu}{D}\right) \\ \frac{d\varepsilon}{d \ln D} &= -\varepsilon + g^2\varepsilon F_1\left(\frac{\mu}{D}\right) + g^2F_2\left(\frac{\mu}{D}\right) \end{aligned} \quad (18)$$

with $F_{1,2}(y) = |1+y|^r \pm 2|1-y|^r$. The last term in $d\varepsilon/d \ln D$ describes the level shift due to the real part of the bath Green's function. A detailed discussion of these equations has been given in Ref. [50], showing that the asymmetric nature of the critical theory induces a strong asymmetry between the two signs of μ in $T_K(\mu)$. In fact, negative μ drives the near-critical system directly into the screened phase, whereas positive μ first induces a crossover to a spin-1/2 moment which is subsequently screened via a conventional Kondo effect. For $r < 1$, where the ACR fixed point is interacting, the scaling prediction holds with $T_K = \kappa_{\pm}|\mu|$ for $\mu \gtrless 0$. In contrast, at the upper critical dimension, $r = 1$, $T_K = \kappa_-|\mu|$ continues to hold for $\mu < 0$, while for $\mu > 0$ logarithmic corrections and Kondo logarithms conspire such that $T_K \propto |\mu|^x$ where $x \approx 2.6$ is a *universal* exponent.

This quantum critical particle-hole asymmetry of $T_K(\mu)$ pertains to the off-critical situation as well. This is nicely seen in the numerical results, Fig. 6b, obtained for a realistic graphene DOS: There is not only asymmetric behaviour for $J_0 \lesssim J_c$, but also the minimum of $T_K(\mu)$ for $J_0 > J_c$ is *not* found at $\mu = 0$ but somewhat away from it.

3.6. Practical consequences for Kondo screening in graphene

Based on the analysis presented so far, we can now specify theoretical predictions for the screening of Kondo impurities in graphene. The half-metallic energy dependence of the graphene DOS implies that Kondo screening tends to be weaker than in conventional metals, implying smaller T_K , and that the single-parameter scaling known from the metallic Kondo problem [2] will in most cases *not* apply. Such unconventional multi-scale crossovers have been studied explicitly [50, 51], also in the presence of a quantizing orbital field [52].

The absence of single-parameter scaling may in fact complicate the unambiguous identification of the Kondo effect – note that typically the scaling of the susceptibility or the resistivity correction has been used to argue in favor of Kondo screening. We believe that, instead, the doping dependence of T_K , the latter extracted, e.g., from the peak width of a tunneling spectrum, can be used as a key indicator of Kondo screening: T_K will strongly vary with doping, with a minimum near charge neutrality.

A concrete prediction of T_K requires a microscopic modelling for the specific type of impurity, which would yield the hybridization and interaction terms of an Anderson

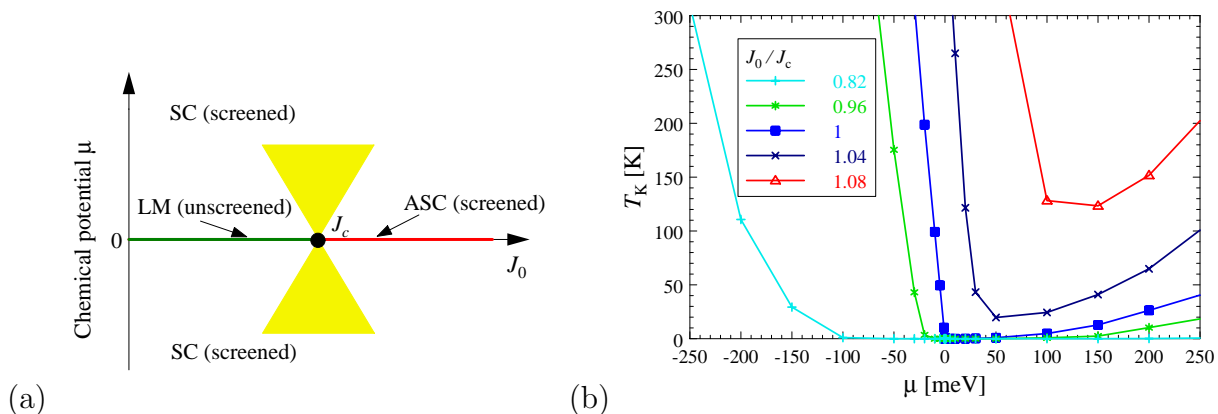


Figure 6. (a) Phase diagram for the pseudogap Kondo problem for $r = 1$ in the presence of finite chemical potential μ . A quantum phase transition between LM and ASC exist in the charge-neutral case, $\mu = 0$, whereas the local moment undergoes Kondo screening for all $\mu \neq 0$. The shaded region is influenced by quantum criticality, with $T_K(\mu)$ following a power law, for details see text and Ref. [50]. (b) NRG results [50] for the Kondo temperature T_K as function of μ for different values of the Kondo coupling J_0 , calculated for a DOS appropriate for Co on graphene [12] where $J_c \approx 4.3$ eV.

impurity model. As discussed in Sec. 2, at present there are considerable uncertainties in these parameters for all relevant impurities. Nevertheless, one may use the ab-initio results for the hybridization function of a Co adatom with $S = 1/2$ in an h position [12] (which should apply to NiH as well) to numerically calculate T_K within an effective Kondo model. Results obtained using NRG have been presented in Ref. [50] and are reproduced in Fig. 6b. The strong μ dependence and the pronounced electron-hole asymmetry of $T_K(\mu)$ are apparent. At $J_0 = J_c$ the linear and power-law behaviours of $T_K(\mu)$, advertised in Sec. 3.5, are nicely visible. Comments on numbers are in order: (i) Due to the uncertainty in the Coulomb interaction U , the effective Kondo coupling J_0 is not known to a good accuracy. Therefore, any *prediction* of T_K , in particular near charge neutrality, comes with excessively large error bars. (ii) In the model leading to Fig. 6b, we have assumed SU(2) symmetry. However, according to Ref. [12], the Co impurity has an approximate SU(4) symmetry which is broken down to SU(2) on a scale of 60 meV. Therefore, the high-energy flow of the Kondo coupling will differ for the two models, such that the critical coupling J_c for Co in this $S = 1/2$ state is predicted to be 2.2 eV, approximately matching the estimate in Ref. [12].

Thermodynamic observables like the impurity contributions to susceptibility, entropy, and specific heat have been calculated for some parameter sets in Refs. [12, 50, 51], but are difficult to measure in the limit of dilute impurities.

3.7. STM and quasiparticle interference

Conduction-electron scattering off impurities can be probed using STM: Conductance spectra can be recorded at/near the impurity site and as function of the distance to the

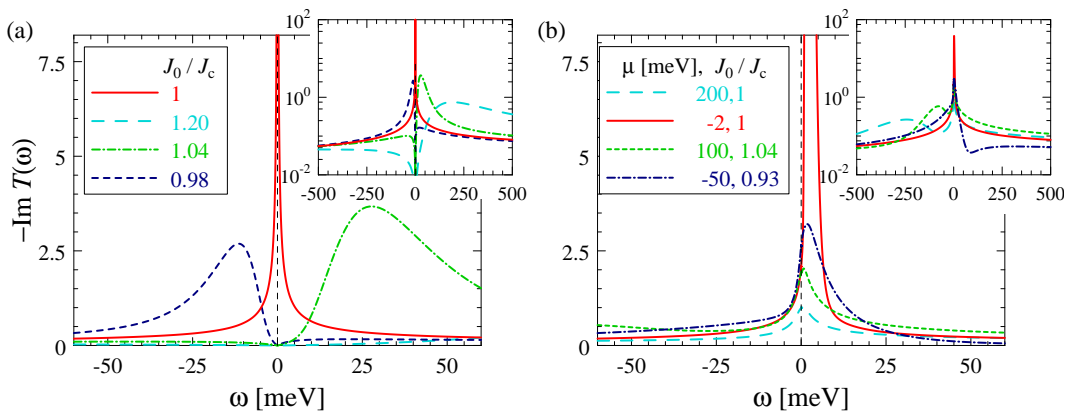


Figure 7. NRG results for the impurity spectral function for different values of the Kondo coupling J_0 , calculated for a DOS appropriate for Co on graphene [12] where $J_c \approx 4.3$ eV. (a) Charge-neutral case $\mu = 0$. (b) Finite μ ; here all parameter sets yield a T_K between 20 and 30 K [50]. The insets show the same data for a larger energy range and on a logarithmic intensity scale.

impurity. In particular, spatial variations in the local DOS, $\rho(\vec{r}, \omega)$, can be interpreted in terms of impurity-induced energy-dependent Friedel oscillations, so-called quasiparticle interference (QPI). Analyzing QPI spectra using models of elastic scattering allows to extract information on both the host band structure and the nature of the impurity.

For graphene, the initial experiments of Manoharan [53] have triggered a number of theoretical studies of local spectra [43, 51, 54, 55, 56] and the expected QPI signal [12, 13, 15]. A striking feature of the Kondo effect in charge-neutral graphene is that impurity spectral density is not peaked *at* the Fermi level, but away from it, with vanishing spectral weight at E_F [51, 57], except for $J_0 = J_c$, see Fig. 7a. In the doped case, single-parameter scaling is again violated for a large range of parameters [50, 51], but the spectrum returns to being dominated by a peak near the Fermi level, Fig. 7b. We note, however, that a detailed comparison between theory and experiment is lacking to date.

4. Experiments and open issues

Despite numerous attempts to create and study Kondo impurities during several years of graphene research, the amount of experimental data is still somewhat limited. Both magnetic adatoms and vacancies have been considered, but clear-cut observations which unambiguously verify available theories have not been reported to our knowledge. We start by summarizing the most prominent experiments, and then discuss issues which might contribute to complicate the interpretation of the data.

4.1. Experiments

4.1.1. Adatoms. Isolated Co adatoms placed on top of a graphene sheet have been studied using STM in Refs. [53, 58]. Ref. [53] employed a conducting SiC substrate

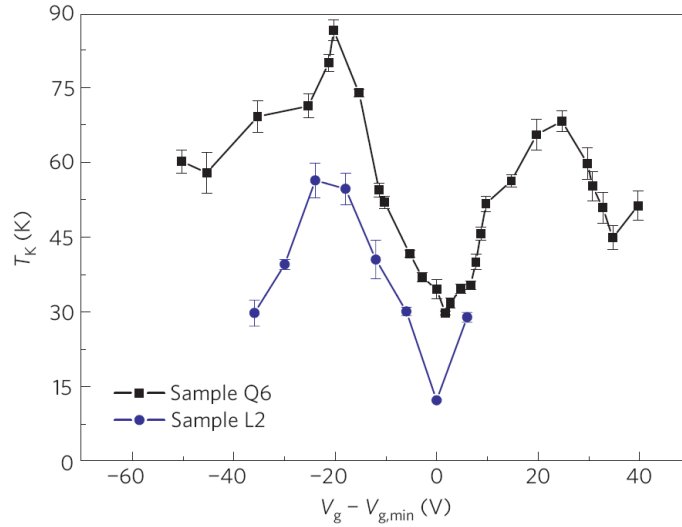


Figure 8. Kondo temperature T_K for vacancy moments in irradiated graphene for two different samples as function of the gate voltage which controls the carrier concentration [59]; $V_{g,min}$ corresponds to charge-neutral case, i.e. the chemical potential located at the Dirac point. The T_K values have been extracted from the temperature dependence of the electrical resistivity (taken from Ref. [59]).

which shifts the chemical potential to roughly $\mu = 0.25$ eV. Spectral signatures of Kondo screening were observed, with $T_K \approx 15$ K, including the expected splitting of the Kondo peak upon application of a magnetic field. Surprisingly, T_K was almost identical for Co atoms placed on the t and h positions of a carbon hexagon, Fig. 2a. For Co in the h position, the energy dependence of the small-bias conductance was interpreted in terms of a two-channel Kondo (2CK) effect, whereas single-channel Kondo (1CK) behaviour was found for Co in a t position.

In contrast, Ref. [58] worked with an insulating SiO_2 substrate which allowed for gate tuning of the chemical potential. Here, clear-cut Kondo signatures were not observed, instead the spectral features mainly reflected charging effects and vibrational excitations.

4.1.2. Defects. In a second group of experiments, point defects within the graphene sheet were created either by irradiation [59, 60], with estimated defect densities ranging from 10^{-5} [59] to 0.1 [60] per C atom, or by depositing fluorine adatoms [60, 61]. In the case of irradiation, it is believed that the main defects are carbon vacancies.

Ref. [59] studied magnetotransport through an irradiated graphene sample placed on a Si substrate and found a resistivity increase at low temperatures combined with negative magnetoresistance, consistent with Kondo screening. Using extensive fits of $\rho(T)$ to the standard theory of the metallic Kondo effect, T_K was found to vary between 30 and 90 K for estimated chemical potentials within $[-0.3 \text{ eV}, 0.3 \text{ eV}]$, see Fig. 8. Such a T_K variation appears rather small compared to that expected within a pseudogap Kondo model, see Sec. 3.6 and Fig. 6. Also, it is surprising that the transport data could be

fitted to theoretical results for metallic Kondo screening even near neutrality where standard single-parameter scaling is not expected due to strong energy dependence of the host DOS. Despite interesting proposals and ideas [62, 63], we feel that a convincing theoretical explanation for the results of Ref. [59] is missing to date. *

Ref. [60] aimed at quantifying defect-induced magnetism in graphene laminates, utilizing magnetization measurements away from the dilute limit. For both fluorine adatoms and vacancies, paramagnetic behaviour of spin-1/2 moments was detected. The measured magnetic moment per defect was between 0.1 and $0.4 \mu_B$ in the vacancy case, possibly consistent with one spin-1/2 per vacancy in the dilute limit (due to uncertainties in estimating the vacancy density). For fluorinated graphene the magnetic moment per adatom was only $10^{-3} \mu_B$ – this extremely small value was ascribed to adatom clustering, such that only larger clusters contribute one spin- $\frac{1}{2}$. In these experiments, neither magnetic order nor signatures of Kondo screening were detected down to 2 K.

Finally, Ref. [61] investigated weak-localization physics in gated graphene with fluorine adatoms with dilute concentrations of order 10^{-4} . The results of the transport measurements were interpreted in terms of suppressed weak localization due to spin-flip scattering from fluorine-generated moments, but the Kondo temperature was estimated to be as small as 0.01 K for carrier densities of $0.6 \times 10^{12}/\text{cm}^2$. Such a low T_K would imply a very small magnetic coupling, $J \sim 5$ meV, between the fluorine-induced moments and the Dirac electrons of graphene, possibly consistent with the absence of both magnetic order and screening as measured in Ref. [60].

4.2. One-channel vs. two-channel Kondo screening

The two-channel Kondo (2CK) effect emerges if a magnetic impurity is coupled symmetrically to two equivalent screening channels of conduction electrons, such that a standard Kondo singlet is unstable [65]. Instead, the low- T behaviour is then governed by a non-trivial intermediate-coupling fixed point with non-Fermi-liquid properties.

2CK physics being relevant for graphene has been proposed theoretically in Refs. [14, 44, 49], based on the idea that the electrons in the two valleys, i.e., near K and K' , could form independent screening channels. The resulting pseudogap 2CK model displays an interesting interplay of pseudogap Kondo physics and the non-Fermi liquid behaviour of the 2CK effect and has been studied in Refs. [21, 66]. However, an analysis of possible microscopic models for graphene impurities suggests that unavoidable inter-valley scattering will invariably couple the two screening channels such that single-channel Kondo screening prevails at least at low energies and temperatures [14], i.e. below a crossover scale $T_{1\text{CK}}$. For well localized magnetic moments, inter-valley scattering is strong resulting in $T_{1\text{CK}} \sim T_K$, such that there is unlikely to be an intermediate regime of 2CK screening.‡ The interpretation of STM data in terms of

* The Kondo interpretation of the transport data of Ref. [59] has been questioned in Ref. [64], where it was instead proposed that electron–electron interactions in the presence of disorder are responsible for the logarithmic resistivity increase at low temperature.

‡ A conventional single-orbital Anderson model cannot lead to 2CK behavior on general grounds [67].

a 2CK effect in Ref. [53] is therefore puzzling.

4.3. Influence of bulk electron-electron interaction

The standard analysis of Kondo models assumes non-interacting host electrons, justified by the assumption of Fermi-liquid behavior and the associated screening of Coulomb interactions [2]. However, in charge-neutral graphene screening is less efficient: The leading interaction effect is a logarithmic upward renormalization of the Fermi velocity, such that the DOS is suppressed compared to the non-interacting $|\omega|$ result by a multiplicative logarithm [68, 69]. This will lead to a further suppression of the Kondo temperature and to a modification of the logarithmic corrections at the critical point of the $r = 1$ pseudogap Kondo problem [37, 50], but otherwise not qualitatively alter the behavior. Away from charge neutrality, the Coulomb interaction is screened, and its effects are minor similar to standard Fermi liquids.

4.4. Influence of electron-hole puddles

A serious complication for quantitative comparisons between theory and experiment, in particular for graphene sheets near charge neutrality, is the presence of electronic inhomogeneities, known as electron-hole puddles [70, 71]. These puddles can be understood as spatial variations of the local carrier concentration or, equivalently, of the local Dirac-point energy, with the characteristic length scale (or puddle size) of 10–20 nm. While the origin of these puddles is under debate [71, 72, 73], a plausible explanation is the influence of charged defects in the substrate.

In the context of Kondo impurities, these puddles imply a spatial variation of the local DOS, which itself determines the local Kondo temperature. Thus, a distribution of Kondo temperatures will be present in a sample with multiple impurities. Importantly, different macroscopic observables will be dominated by different parts of this distribution: Whereas the magnetic susceptibility will be dominated by weakly screened (i.e. low- T_K) moments, the electric resistivity receives mainly contributions from strongly screened (i.e. high- T_K) moments. For metallic systems with a broad distribution of Kondo temperatures, non-Fermi-liquid behaviour may arise, as has been discussed in the framework of so-called Kondo-disorder models [74, 75].

For graphene, an interesting question is whether Kondo disorder could explain the weak gate-voltage dependence of the transport- T_K in the experiment of Ref. [59]. However, we believe that this is unlikely to be the case: Weak disorder is insufficient to significantly modify the $T_K(\mu)$ dependence, whereas strong disorder would yield a broad T_K distribution which appears incompatible with the fact that the transport data [59] could be well described by the universal metallic Kondo behaviour with a single T_K .

4.5. Multiple impurities: RKKY interaction and magnetic order

In samples with a non-vanishing concentration of magnetic impurity moments, the issue of impurity-induced order becomes relevant, with the coupling between the moments mediated by conduction electrons via the Ruderman-Kittel-Kasuya-Yosida (RKKY) interaction. For magnetic moments in metals, magnetic order sets in only at rather high concentrations (typically 20% or more), because otherwise Kondo screening is likely to prevail. This can be different in semiconductors, and indeed semiconductors doped with magnetic ions display ferromagnetism with Curie temperatures above 100 K [76], possibly important for spintronics applications.

For graphene, the RKKY interaction has been discussed theoretically [77, 78, 79, 80]. For charge-neutral graphene, the oscillations with distance r typical of RKKY interactions are absent, such that the interaction is strictly ferromagnetic for moments on the same sublattice and antiferromagnetic for moments on different sublattices, in both cases falling off as $1/r^3$. Thus, an inhomogeneous but unfrustrated antiferromagnetic ground state can be expected for randomly placed moments. Such order is predicted to persist at finite temperature even in this 2d situation due to the long-range nature of the RKKY interaction [81]. Departing from charge neutrality, a crossover to standard metallic behaviour is expected.

The competition of RKKY-induced order with Kondo screening has not been studied in detail, but it is plausible that most considerations for magnetic moments in metals apply: Away from charge neutrality, one expects a quantum phase transition between a Fermi liquid with screened moments and an ordered state which is either antiferromagnetic or spin-glass-like. As with other quasi-2d metals, the nature of this phase transition is an open problem [82, 83, 84]. In the neutral case, the transition is between a semimetal and a magnetic insulator – such a transition has been investigated in the absence of quenched disorder [85], but the effect of randomness due to moment disorder has not been studied. Experimentally, impurity-induced magnetic order in graphene has not been observed to our knowledge (see e.g. Ref. [60] for an attempt).

4.6. Summary

Studying magnetic moments in graphene holds the prospect of observing exciting phenomena, such as Kondo physics beyond one-parameter scaling, single-impurity quantum criticality and associated local non-Fermi-liquid behaviour, magnetic order from dilute moments, and lattice quantum criticality in strictly two dimensions. While for most of these, a theoretical framework is available, experimental data is scarce and more experimental activities are clearly called for.

5. Outlook: Beyond graphene

The Kondo effect in graphene is related to a variety of other quantum impurity problems. This section will highlight the most important connections.

5.1. Kondo impurities in unconventional superconductors

The pseudogap Kondo problem was first discussed [31] in the context of magnetic impurities in unconventional superconductors. For BCS states with nodes in the superconducting gap function, the density of states of Bogoliubov quasiparticles vanishes algebraically as $\omega \rightarrow 0$. Moreover, a locally coupled impurity, $V_k = V$ in Eq. (5), is not directly influenced by pairing, because the local anomalous Green's function vanishes in an unconventional superconductor [86]. Then, the Kondo problem in such a superconductor is equivalent to the pseudogap Kondo problem described in Sec. 3, with a $|\omega|^r$ density of states at low energies and $r = 1$ ($r = 2$) for d -wave (p -wave) superconductors. Importantly, the Fermi energy is always pinned to charge neutrality, i.e. the crossovers described in Sec. 3.5 cannot be accessed.

A clear-cut experimental observation of Kondo screening in unconventional superconductors ideally requires $T_K \lesssim T_c$, with T_c being the superconducting transition temperature, together with the ability to tune either the host gap or the Kondo coupling. While the latter can be efficiently varied in nanostructures with quantum dots, we are not aware of corresponding experimental results, likely because of the lack of suitable unconventional superconductors as lead materials. In bulk superconductors with impurities, signatures of Kondo screening have been detected in NMR measurements on Zn-doped high- T_c cuprates of the $\text{YBa}_2\text{Cu}_3\text{O}_y$ family [87, 88]. Similarly, STM experiments on $\text{Bi}_2\text{Sr}_2\text{CaCu}_2\text{O}_{8+\delta}$ have detected large low-energy conductance peaks near Zn impurities [89], which subsequently have been interpreted in terms of a Kondo resonance [41, 57].^{††} It should be noted, however, that other interpretations for the STM data have been put forward as well [89, 90, 91], and a concise picture for impurity effects in cuprates has not yet emerged.

5.2. Kondo impurities on the surface of topological insulators

The 2d surface states of 3d topological insulators (TI) admit a low-energy description in terms of a Dirac equation. The resulting electronic properties are therefore similar to that of graphene, with a few important differences: (i) there is a single Dirac cone (or, more generally, an odd number) per surface, and (ii) the role of the pseudospin (or sublattice) in the graphene case is taken by the physical spin, such that TI surface states display spin-momentum locking, and there is no additional spin degeneracy.

The physics of Kondo impurities in this setting has been analyzed theoretically in a number of papers recently [92, 93, 94]. The main conclusion is that, despite the non-trivial topological structure of the TI surface states, the corresponding local Kondo problem for a spin $S = 1/2$ impurity can be mapped onto the standard pseudogap Kondo model of Sec. 3. Consequently, strong deviations from conventional, i.e. metallic, Kondo screening are expected once the Fermi level is tuned close to the Dirac-point energy of the

^{††}For cuprates, it has been assumed that the non-magnetic Zn ion induces a magnetic moment by a mechanism of dimer breaking, as happens in spin-gapped magnets such as spin ladders.

surface states. Experimentally, magnetic moments on TI surfaces have been investigated in a few papers [95, 96, 97], but not in the dilute regime with focus on Kondo screening.

5.3. Kondo physics in spin liquids

A somewhat different, but still overlapping, topic is the physics of magnetic impurities embedded in quantum magnets. The closest relation to the graphene Kondo problem is found for host magnets without semiclassical long-range order, but still a gapless spectrum of excitations. Two interesting cases will be discussed in the following.

In quantum-critical magnets, located near a zero-temperature transition between an antiferromagnet and a paramagnet, the elementary host excitations are spin-1 critical magnons which interact with the impurity spin via a Yukawa-type (i.e. three-point) coupling. As a result, true Kondo singlet formation is not possible. In dimensions $1 < d < 3$, RG studies have predicted a partial screening of the spin, described by a non-trivial intermediate-coupling fixed point [98, 99]. In $d = 2$ this prediction has been verified numerically [100].

Magnetic impurities in gapless spin-liquid phases are more akin to Kondo problems: Here the host excitations are typically spin-1/2 spinons coupled to a U(1) and Z_2 gauge field. The spinons couple to the impurity spin with a Kondo-like (i.e. four-point) interaction. The physics depends on the nature of the spinons, and a few cases have been discussed in the literature. Linearly dispersing bosonic spinons yield a rich phase diagram, with a variety of possible $T = 0$ phases, including the possibility of full Kondo screening, and quantum phase transitions [45]. In contrast, fermionic spinons lead to physics similar to standard Kondo expectations: In the presence of a spinon Fermi surface, the impurity spin gets always screened at low T [101]. In the case of 2d Dirac spinons of an algebraic spin liquid, a quantum phase transition not unlike that of the pseudogap Kondo problem, Sec. 3, emerges [40, 102, 103]. However, it should be noted that the influence of gauge fields beyond perturbation theory has been neglected in the published treatments.

Acknowledgments

We thank A. Castro Neto, P. Coleman, P. Cornaglia, K. Ingersent, H. Manoharan, A. Mitchell, A. Rosch, B. Uchoa, and T. Wehling for illuminating discussions as well as F. B. Anders, R. Bulla, S. Florens, M. Kircan, A. Polkovnikov, S. Sachdev, I. Schneider, and M. Zwiebler for collaborations on these and related topics. This research was supported by the DFG via SFB 608, SFB/TR 12, FOR 960, GRK 1621, and the Emmy-Noether programme (FR 2627/3-1).

References

- [1] Kondo J 1964 *Prog. Theor. Phys.* **32** 37

- [2] Hewson A C 1997 *The Kondo Problem to Heavy Fermions* (Cambridge: Cambridge University Press).
- [3] Novoselov K S, Geim A K, Morozov S V, Jiang D, Zhang Y, Dubonos S V, Grigorieva I V and Firsov A A 2004 *Science* **306** 666
- [4] Novoselov K S, Geim A K, Morozov S V, Jiang D, Katsnelson M I, Grigorieva I V, Dubonos S V and Firsov A A 2005 *Nature* **438** 197
- [5] Castro Neto A H, Guinea F, Peres N M R, Novoselov K S and Geim A K 2009 *Rev. Mod. Phys.* **81** 109
- [6] Das Sarma S, Adam S, Hwang E H and Rossi E 2011 *Rev. Mod. Phys.* **83** 407
- [7] Vojta M 2006 *Phil. Mag.* **86** 1807
- [8] Wallace P R 1947 *Phys. Rev.* **71** 622
- [9] Anderson P W 1961 *Phys. Rev.* **124** 41
- [10] Manoharan H C, Lutz C P and Eigler D M 2000 *Nature* **403** 512
- [11] Costi T A, Bergqvist L, Weichselbaum A, von Delft J, Micklitz T, Rosch A, Mavropoulos P, Dederichs P H, Mallet F, Saminadayar L, Bauerle C 2009 *Phys. Rev. Lett.* **102** 056802
- [12] Wehling T O, Balatsky A V, Katsnelson M I, Lichtenstein A I and Rosch A 2010 *Phys. Rev. B* **81** 115427
- [13] Uchoa B, Yang L, Tsai S-W, Peres N M R and Castro Neto A H 2009 *Phys. Rev. Lett.* **103** 206804
- [14] Zhu Z-G, Ding K-H and Berakdar J 2010 *EPL* **90** 67001
- [15] Uchoa B, Yang L, Tsai S-W, Peres N M R and Castro Neto A H 2011 *preprint* arXiv:1105.4893
- [16] Uchoa B, Rappoport T G and Castro Neto A H 2011 *Phys. Rev. Lett.* **106** 016801; *Phys. Rev. Lett.* **106** 159901(E)
- [17] Wehling T O, Lichtenstein A I and Katsnelson M I 2011 *Phys. Rev. B* **84** 235110
- [18] Jacob D and Kotliar G 2010 *Phys. Rev. B* **82**, 085423
- [19] Rudenko A N, Keil F J, Katsnelson M I and Lichtenstein A I 2012 *preprint* arXiv:1206.1222
- [20] Uchoa B, Kotov V N, Peres N M R and Castro Neto A H 2008 *Phys. Rev. Lett.* **101** 026805
- [21] Gonzalez-Buxton C and Ingersent K 1998 *Phys. Rev. B* **57** 14254
- [22] Nai R R, Sepioni M, Tsai I-L, Lehtinen O, Keinonen J, Krasheninnikov A V, Thomson T, Geim A K and Grigorieva I V 2012 *Nature Phys.* **8** 199
- [23] McCreary K M, Swartz A G, Han W, Fabian J and Kawakami R K 2012 *preprint* arXiv:1206.2628
- [24] Pereira V M, Guinea F, Lopes dos Santos J M B, Peres, N M R and Castro Neto A H 2006 *Phys. Rev. Lett.* **96** 036801
- [25] Yazyev O V and Helm L 2007 *Phys. Rev. B* **75** 125408
- [26] Haase P, Fuchs S, Pruschke T, Ochoa H and Guinea F 2011 *Phys. Rev. B* **83** 241408(R)
- [27] Sofo J O, Usaj G, Cornaglia P S, Suarez A M, Hernandez-Nieves A D and Balseiro C A 2012 *Phys. Rev. B* **85** 115405
- [28] Palacios J J and Yndurain F 2012 *Phys. Rev. B* **85** 245443
- [29] Cazalilla M A, Iucci A, Guinea F and Castro Neto A H 2012 *preprint* arXiv:1207.3135
- [30] Vojta M and Bulla R 2002 *Eur. Phys. J B* **28** 283
- [31] Withoff D and Fradkin E 1990 *Phys. Rev. Lett.* **64** 1835
- [32] Hentschel M and Guinea F 2007 *Phys. Rev. B* **76** 115407
- [33] Bulla R, Pruschke T and Hewson A C 1997 *J. Phys.: Condens. Matter* **9** 10463
- [34] Bulla R, Glossop M T, Logan D E and Pruschke T 2000 *J. Phys.: Condens. Matter* **12** 4899
- [35] Ingersent K and Si Q 2002 *Phys. Rev. Lett.* **89** 076403
- [36] Vojta M and Fritz L 2004 *Phys. Rev. B* **70** 094502
- [37] Fritz L and Vojta M 2004 *Phys. Rev. B* **70** 214427
- [38] Read N and Newns D M 1983 *J. Phys. C* **16** 3273
- [39] Ingersent K and Si Q 1998 *preprint* arXiv:cond-mat/9810226 (unpublished)
- [40] Cassanello C R and Fradkin E 1996 *Phys. Rev. B* **53** 15079
- [41] Polkovnikov A, Sachdev S and Vojta M 2001 *Phys. Rev. Lett.* **86** 296

- [42] Polkovnikov A 2002 *Phys. Rev. B* **65** 064503
- [43] Zhuang H B, Sun Q-f and Xie X C 2009 *EPL* **86** 58004
- [44] Dell'Anna L 2010 *J. Stat. Mech.* P01007
- [45] Fritz L, Florens S and Vojta M 2006 *Phys. Rev. B* **74** 144410
- [46] Glossop M T, Kirchner S, Pixley J H and Si Q 2011 *Phys. Rev. Lett.* **107** 076404
- [47] Pixley J H, Kirchner S, Ingersent K and Si Q 2011 *preprint* arXiv:1108.5227
- [48] Fritz L 2006 *PhD thesis* Universität Karlsruhe
- [49] Sengupta K and Baskaran G 2007 *Phys. Rev. B* **77** 045417
- [50] Vojta M, Fritz L and Bulla R 2010 *EPL* **90** 27006
- [51] Cornaglia P S, Usaj G and Balseiro C A 2009 *Phys. Rev. Lett.* **102** 046801
- [52] Dora B and Thalmeier P 2007 *Phys. Rev. B* **76** 115435
- [53] Manoharan H C 2011 *Bulletin of the American Physical Society* BAPS.2011.MAR.P2.1 (unpublished)
- [54] Wehling T O, Dahal H P, Lichtenstein A I, Katsnelson M I, Manoharan H C and Balatsky A V 2010 *Phys. Rev. B* **81** 085413
- [55] Saha K, Paul I and Sengupta K 2010 *Phys. Rev. B* **81** 165446
- [56] Zhu Z-G and Berakdar J 2011 *Phys. Rev. B* **84** 165105
- [57] Vojta M and Bulla R 2001 *Phys. Rev. B* **65** 014511
- [58] Brar V W, Decker R, Solowan H-M, Wang Y, Maserati L, Chan K T, Lee H, Girit C O, Zettl A, Louie S G, Cohen M L and Crommie M F 2011 *Nature Phys.* **7** 43
- [59] Chen J-H, Li L, Cullen W G, Williams E D and Fuhrer M S 2011 *Nature Phys.* **7** 535
- [60] Nair R R, Sepioni M, Tsai I-L, Lehtinen O, Keinonen J, Krasheninnikov A V, Thomson T, Geim A K and Grigorieva I V 2012 *Nature Phys.* **8** 199
- [61] Hong X, Zou K, Wang B, Cheng S-H and Zhu J 2012 *Phys. Rev. Lett.* **108** 226602
- [62] Chao S-P and Aji V 2011 *Phys. Rev. B* **83** 165449
- [63] Kanao T, Matsuura H and Ogata M 2012 *J. Phys. Soc. Jpn.* **81** 063709
- [64] Jobst H and Weber H B 2012 *Nature Phys.* **8** 352; Chen J-H *et al.* 2012 *Nature Phys.* **8** 353
- [65] Nozières P and Blandin A 1980 *J. de Physique* **41** 193
- [66] Schneider I, Fritz L, Anders F B, Benlagra A and Vojta M 2011 *Phys. Rev. B* **84** 125139
- [67] Coleman P and Tselik A M 1998 *Phys. Rev. B* **59** 12757
- [68] Gonzalez J, Guinea F and Vozmediano M A H 1994 *Nucl. Phys. B* **424** 595
- [69] Elias D C, Gorbachev R V, Mayorov A S, Morozov S V, Zhukov A A, Blake P, Ponomarenko L A, Grigorieva I V, Novoselov K S, Guinea F and Geim A K 2011 *Nature Phys.* **7** 701
- [70] Martin J, Akerman N, Ulbricht G, Lohmann T, Smet J H, von Klitzing K and Yacoby A 2008 *Nature Phys.* **4** 144
- [71] Zhang Y, Brar V W, Girit C, Zettl A and Crommie M F 2009 *Nature Phys.* **5** 722
- [72] Schubert G and Fehske H 2012 *Phys. Rev. Lett.* **108** 066402
- [73] Gibertini M, Tomadin A, Guinea F, Katsnelson M I and Polini M 2012 *Phys. Rev. B* **85** 201405(R)
- [74] Miranda E, Dobrosavljevic V and Kotliar G 1996 *J. Phys. Cond. Matter* **8** 9871
- [75] Castro Neto A H and Jones B 2000 *Phys. Rev. B* **62** 14975
- [76] Jungwirth T, Sinova J, Malek J, Kucera J and MacDonald A H 2006 *Rev. Mod. Phys.* **78** 809
- [77] Vozmediano M A H, Lopez-Sancho M P, Stauber T and Guinea F 2005 *Phys. Rev. B* **72** 155121
- [78] Saremi S 2007 *Phys. Rev. B* **76** 184430
- [79] Brey L, Fertig H A and Das Sarma S 2007 *Phys. Rev. Lett.* **99** 116802
- [80] Black-Schaffer A M 2010 *Phys. Rev. B* **80** 205416
- [81] Fabritius T, Lafforencie N and Wessel S 2010 *Phys. Rev. B* **82** 035402
- [82] von Löhneysen H, Rosch A, Vojta M and Wölfle P 2007 *Rev. Mod. Phys.* **79** 1015
- [83] Gegenwart P, Si Q and Steglich F 2008 *Nature Phys.* **4**, 186
- [84] Sachdev S, Metlitski M A and Punk M 2012 *Journal of Physics: Cond. Matter* **24**, 294205
- [85] Herbut I F 2006 *Phys. Rev. Lett.* **97** 146401
- [86] Fritz L and Vojta M 2005 *Phys. Rev. B* **72** 212510

- [87] Bobroff J, MacFarlane W A, Alloul H, Mendels P, Blanchard N, Collin G and Marucco J-F 1999 *Phys. Rev. Lett.* **83** 4381
- [88] Bobroff J, Alloul H, MacFarlane W A, Mendels P, Blanchard N, Collin G and Marucco J-F 2001 *Phys. Rev. Lett.* **86** 4116
- [89] Pan S H, Hudson E W, Lang K M, Eisaki H, Uchida S and Davis J C 2000 *Nature* **403** 746
- [90] Martin I, Balatsky A V and Zaanen J 2002 *Phys. Rev. Lett.* **88**, 097003
- [91] Balatsky A V, Vekhter I and Zhu J-X 2006 *Rev. Mod. Phys.* **78** 373
- [92] Feng X-Y, Chen W-Q, Gao J-H, Wang Q-H and Zhang F C 2010 *Phys. Rev. B* **81** 235411
- [93] Zitko R 2010 *Phys. Rev. B* **81** 241414
- [94] Tran M-T and Kim K-S 2010 *Phys. Rev. B* **82** 155142
- [95] Ye M, Ereameev S V, Kuroda K, Krasovskii E E, Chulkov E V, Takeda Y, Saitoh Y, Okamoto K, Zhu S Y, Miyamoto K, Arita M, Nakatake M, Okuda T, Ueda Y, Shimada K, Namatame H, Taniguchi M and Kimura A 2012 *Phys. Rev. B* **85** 205317
- [96] Scholz M R, Sanchez-Barriga J, Marchenko M, Varykhalov A, Volykhov A, Yashina L V and Rader O 2012 *Phys. Rev. Lett.* **108** 256810
- [97] Honolka J, Khajetoorians A A, Sessi V, Wehling T O, Stepanow S, Mi J-L, Iversen B B, Schlenk T, Wiebe J, Brookes N, Lichtenstein A I, Hofmann P, Kern K and Wiesendanger R 2011 *preprint* arXiv:1112.4621
- [98] Sachdev S, Buragohain S and Vojta M 1999 *Science* **286** 2479
- [99] Sachdev S and Vojta M 2003 *Phys. Rev. B* **68** 064419
- [100] Höglund K H and Sandvik A W 2007 *Phys. Rev. Lett.* **99** 027205
- [101] Ribeiro P and Lee P A 2011 *Phys. Rev. B* **83** 235119
- [102] Kim K-S and Kim M D 2008 *J. Phys. Cond. Matter* **20** 125206
- [103] Dhochak K, Shankar R and Tripathi V 2010 *Phys. Rev. Lett.* **105** 117201